Universiteit Utrecht

Department of Physics
Department of Mathematics

Bachelor Thesis

Eleonora van den Dungen

Double Bachelor Physics & Mathematics

An Analytical and Numerical Study of the Electric Double Layer in a Cylindrical Nanochannel with a Concentration Gradient

Supervisors:

Prof. dr. R. van Roji
Institute for Theoretical Physics

Prof. dr. ir. J. E. Frank
Mathematic Institute

MSc. W. Boon
Institute for Theoretical Physics

January 15, 2020

Abstract

This work aims to extend the study of the formation of the heterogeneous electric double layer. This electric double layer occurs at the interface of a solution in a channel with a salt concentration difference at either side of the channel and the surface charge of the channel walls. This behaviour is described by the Nernst-Planck, Navier-Stokes and Poisson equations. First a modified Debye length depending on the concentration is derived analytically to take this concentration gradient into account and is used to derive analytical expressions for the electric potential and the fluid velocity. The modelling program COMSOL Multiphysics is used to build a simulation of this system consisting of a concentration gradient over a nanochannel. It is found that at small concentration differences, the in this work derived analytical solutions describe the system very well. However, for large concentration gradients these analytical expressions do no longer hold. Further research needs to be done to understand the behaviour occurring due to a large concentration gradient.

Contents

1 Introduction

As global demand for energy continues to rise, a lot of research is done into a sustainable energy source. One of these sources is a saline gradient in a fluid. This source of energy exists at the interface between bodies of different salinities, primarily at the place where fresh water flows into the ocean [1].
Due to recent rapid developments in technology enables engineering on a nano scale, this energy is potentially available [2]. Reverse electro dialysis is a membrane-based technology which exists to convert this energy into a useful power source. One of the ways this technology can be applied is on the transport of ions in a nanochannel. However, the mechanism behind this electrokinetic transport is not completely understood [3]. Rice and Whitehead were one of the first give a complete analysis of electro-osmotic flow in round capillaries [4]. After this, a lot of works on electrokinetics were published building on their analysis. Due to the fact that non-steady state solutions of the coupled partial differential equation which govern electrokinetic transport are quite complex to solve, most of the studies done until recent focus on the steady state situations [5, 6, 7, 8, 9]. However, developments in the usage of finite element analysis and an rise in computing ability, enables the process of solving a complex non-steady state situation with an numerical approach [10, 11]. This allows for the study of the complete physical behaviour of a system instead of only looking at a theoretic frame. For example in chemistry, finite element modelling is used on a nano pore detector or nanochannels in a cell membrane [12, 13, 14]. This finite element method can be used to gain an insight into the mechanism behind the ionic transport in a nanochannel. To describe the principles governing the fluid flow in a porous membrane with a salinity gradient, a theoretical system is considered.
The theoretical system considered consists of a charged nanochannel with a radius of the orders of nanometres and a length of the orders of micrometers. The channel is connected to two reservoirs. Due to concentration constraints in the interior of the two reservoirs, a concentration gradient is imposed across the system. The system is filled with a solution of symmetrical monovalent electrolyte, of which the ions are modelled as point charges. The concentration constraint and the surface charge result in a inhomogeneous charge distribution in the channel. The electric potential of ions in the electric double layers at the interface between the nano channel wall and the electrolyte will strongly influence the rates of axial ion transport, the streaming potential which is the electric field created by the motion of the ionized fluid along the stationary charged surface and the flow of the bulk.
As the intrinsic heterogeneities of the electric double layer in the channel by an applied salinity gradient make the system very challenging and not well understood, more research needs to be done on these heterogeneities to gain an insight into the behaviour of the diffusio-osmotic currents which result from a concentration gradient [15]. First of all it is required to know how the fluxes react to different linear concentration gradient. This raises the question if it is possible to describe the electric potential for the heterogeneous electric double layer with an analytical expression. Maybe it is possible to find an analytical expression for the fluid velocity field as well, as this combined with the electric potential describes a large part of the fluxes in the system. To find an answer to these questions, a research will be constructed in the following manner. For the research, the concentration difference between the two reservoirs will be the main variable considered. In the theoretical background, the electric double layer will be discussed. Furthermore an expression for the electric potential and velocity field will be derived. The linear relation between the chemical driving force and the fluxes will be discussed as well. Afterwards, a model will be constructed which employs the coupled Poisson, Nernst-Planck and Navier-Stokes equation to describe the diffusio-osmotic flow in a finite charged cylindrical channel. A comparison will be made between the quantities obtained through this numerical model and the derived analytical expressions for the electric potential and velocity field. This method of research is used to see if the numerical model verifies the analytical expressions found in the theory section for a certain regime of concentration gradients and it enables the finding of an answer to the questions raised, which will give a better insight into this system and its intrinsic values.

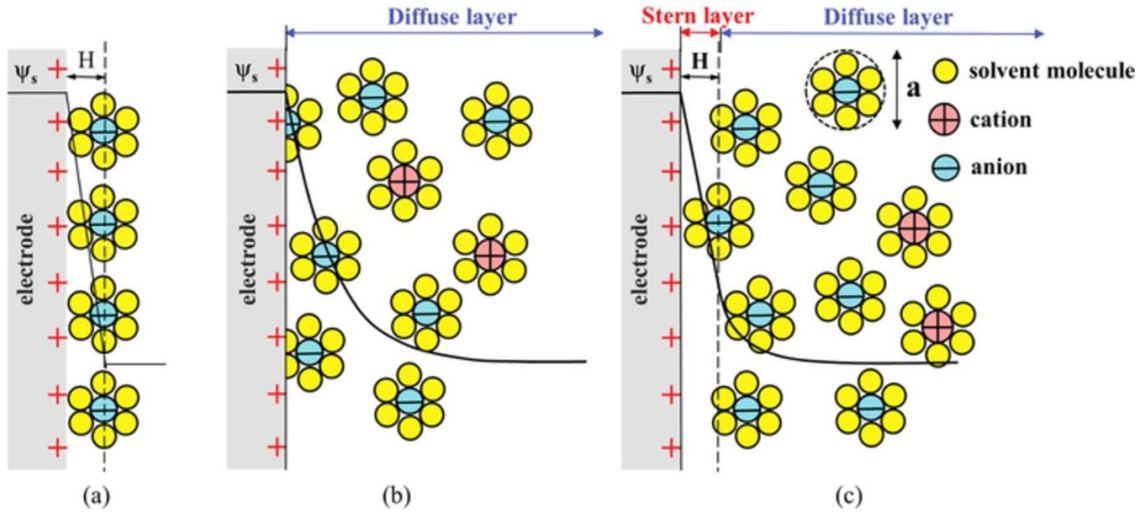

Figure 1: Schematic representation of electrical double layer structures according to (a) the Helmholtz model, (b) the Gouy-Chapman model, and (c) the Gouy-Chapman-Stern model. The double layer distance in the Helmholtz model and the Stern layer thickness are denoted by H while ψ_s is the potential at the electrode surface. [16]

2 Theoretical Background

The theoretical background necessary to understand the flow of particles through a charged nanochannel is given in this section. The driving force considered is a salt concentration gradient. In this section the potential and fluid velocity necessary to describe the three fluxes this driving force induces. These three fluxes are the fluid volume flux, the electric current and the salt flux.

2.1 The Electric Double Layer

This section describes the behaviour of an external object immersed in water. It follows for the main part the discussion by van Roji [17]. This object could be a microscopic nanochannel. Due to the large dielectric constant of water compared to air ($\varepsilon_{water}/\varepsilon_{air} = 78.5$) dissociation of the chemical groups on the surface of the object tends to occur and free ions leave the surface. As a result an net surface charge is created. This net charge attracts counter-ions (ions which charge is opposite to the charge of the surface) and these counter-ions screen the net charge. As a result the counter-ions will not be uniformly spread in the solution. These counter-ions are diffusely distributed close to the surface and will create a charge imbalance close to the surface. This means that the counter-ions are spreading out from a high concentration of counter-ions at the channel surface to the rest of the channel. The typical thickness of this region in which this behaviour happens is called the Debye length. Closer to the surface means that more counter-ions are attracted to the surface and a larger electric potential as a result of this charge imbalance. Several Debye lengths away form the surface, this charge imbalance is very small. At some point an equilibrium is created called the electric double layer. There are several visualisation models for the electric double layer. The one discussed in this work will be the model of Gouy-Chapman for point-like ion particles. Figure 1 gives an overview of the commonly used models.

2.2 The System Under Consideration

Now consider a cylindrical channel with a homogeneous surface with radius R and length L with the axis of the channel pointing in the z-direction. The surface is in contact with an electrolyte. The electrolyte consists of a solvent of temperature T and dielectric constant (relative permittivity) ε_r in the volume V described by $V = \{(r, \phi, z)|0 \leq r \leq R, 0 < \phi \leq 2\pi, -L/2 < z < L/2\} \cup \{(r, \phi, z)|0 \leq r \leq L, 0 < \phi \leq 2\pi, z \leq -L/2 \wedge L/2 \leq z\}$ with r the radial position, z the axial position and ϕ the rotation angle where the first set denotes the

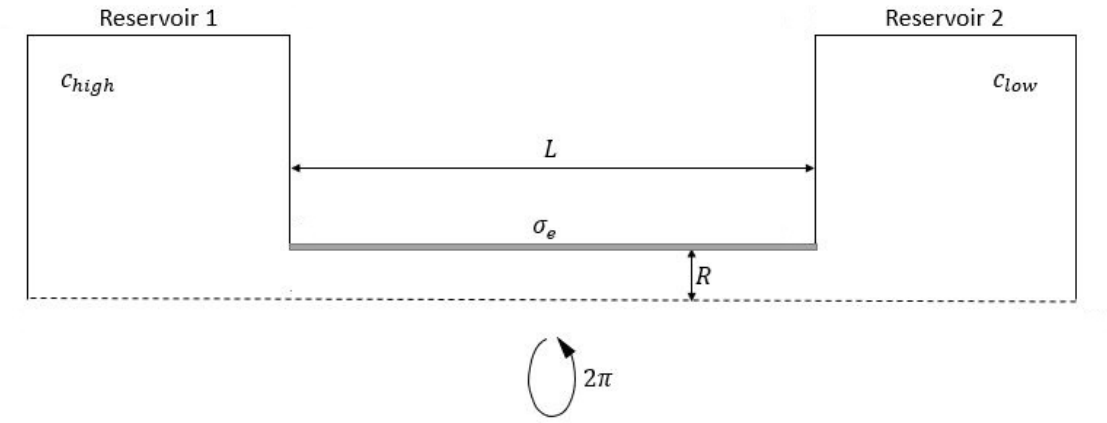

Figure 2: The nanochannel with its surface charge σ_e, length L and radius R connected to two reservoirs with different concentrations c_{high} and c_{low} of the same [1:1] salt. The dashed line represents the channel axis.

collection of points which make up the inside of the nanochannel and the second set the interiors of the two reservoirs. In the solvent are monovalent cations and anions with respective charge $+e$ and $-e$ dissolved with e the elementary charge. The net surface charge is homogeneously distributed over the surface, with the surface charge density given as σ_e. The nanochannel is connected to two large reservoirs filled with the same electrolyte but of different concentrations. Reservoir 1 consists of a higher bulk concentration than that of reservoir 2. The concentration difference between the reservoirs drives the flow of the solvent and the charge through the channel in the axial direction. Figure 2 gives a schematic view of the discussed system. As a result of rotation symmetry the system can be described by its radial and axial position only. All parameters, physical values and their functions are defined on the domain consisting of the inside of the nanochannel and the interiors of the reservoirs.
For an electrolyte subjected to an electric field, the Poisson-Nernst-Planck-Stokes equations can be used to describe the flux of ions through the electrolyte, in the following sections, parts of these equations will be discussed.

2.3 The Nernst-Planck Equation

This section is used to introduce the Nernst-Planck equation for a stationary state. This equation describes the flux of ions under both an ionic concentration gradient and an electric field. The Nernst-Planck equation is defined as [18]

$$0 = -\nabla \cdot \mathbf{j}_i, \tag{1}$$

where the flux $\mathbf{j}_i$ for ionic species $i = \pm$ consists of convective, diffusive and advective flux components. The total flux is given by

$$\mathbf{j}_i = \mathbf{u}c_i - D_i \nabla c_i - D_i z_i c_i \frac{e}{k_B T} \nabla \psi.. \tag{2}$$

The flux due to convection depends on the flow velocity field $\mathbf{u}$ and local concentration $c_i = c_i(r, z)$. Note that this local concentration is a non-negative function. As only a 1:1 electrolyte consisting of monovalent ions with charge $\pm e$ is considered, this can be simplified to c_+ for the cation and c_- for the anion. From here on forward, the subscript $+$ is used to denote the cationic species and the subscript $-$ is used to denote the anionic species. The flux due to advection is a result of the electric field given by the negative gradient of the electric potential $\psi = \psi(r, z)$. This flux depends on the valence of the ionic species $z_\pm = \pm 1$. The diffusivity for the ionic species is given by the positive constant $D_\pm > 0$. The Boltzmann constant is denoted by k_B and the elementary charge by e. The flux due to diffusion is a result the concentration gradient. Equation 1 and 2 show that the fluid flow as a result of a concentration gradient if there is no external potential ($\psi = 0$)

will be constant. An in depth discussion of the electric potential will happen in the next section. The flow velocity field as a result of this electric potential will be discussed later.

2.4 The Potential

To describe the behaviour of the electric double layer, it is necessary to understand the physics and equations governing the local electric potential inside the nanochannel. This will be done in this section. First the Poisson equation will be discussed. Combined with the Boltzmann distribution, this equation will give rise to the Poisson-Boltzmann equation. To find the electric potential a dimensionless potential will be introduced, after which the cylindrical system will be approximated to a planar system to find the solution to the dimensionless potential.

2.4.1 The Poisson-Boltzmann equation

The Poisson equation can be used to describe the characteristics for the electric double layer. The Poisson equation describes the change in electric potential of the electrolyte due to the excess charge over space. For the cylindrical channel this becomes

$$-\nabla^2\psi = \frac{\rho_e}{\varepsilon_0\varepsilon_r}, \tag{3}$$

where ε_r is the dielectric constant of the solvent and ε_0 is the permittivity of free space. The local electric charge density ρ_e is given by

$$\rho_e = eN_A(c_+ - c_-), \tag{4}$$

with N_A being Avogadro's number and $c_\pm$ is denoted in mole per cubic meter. A special notation will be introduced to denote the ion concentration on the channel axis, $c^0_\pm(z) = c_\pm(0,z)$ as due to the different bulk concentrations in the two reservoirs, the concentration of the ions is not uniform along the nanochannel axis. This imposed concentration gradient prevents the system from creating an equilibrium. The Boltzmann distribution model is often used to describe concentrations in an equilibrium state. However the assumptions that the Debye length is much smaller than the distance under which $c^0_\pm(z)$ changes and that there is no radial component to the flow velocity, enables the use of the Boltzmann distribution. The local equilibrium hypothesis can be used to derive this Boltzmann distribution. The local equilibrium hypothesis assumes that a system can be viewed as formed of subsystems where the rules of equilibrium thermodynamics apply. This implies that there is no flux in the radial direction ($\mathbf{j}_\pm \cdot \hat{r} = 0$, with $\hat{r}$ the unit vector in the radial direction). From Equation 2 then follows that

$$\partial_r c_\pm = \mp c_\pm \frac{e}{k_B T}\partial_r\psi. \tag{5}$$

The integration of this gives the same result as the Boltzmann distribution for only electric work. The Boltzmann distribution is given as

$$c_\pm(r,z) = c^0_\pm(z) \cdot e^{\frac{-W_\pm}{k_B T}}, \tag{6}$$

in which $W_\pm$ is the work required to move an ion with charge $\pm$ closer to the charged surface from the channel axis. In the case of the work consisting only of electric work it can be rewritten as $W_\pm(r,z) = \pm(e\psi(r,z) - e\psi_0(z))$ in which $\psi_0(z)$ denotes the potential on the channel axis. The concentration can be given as

$$c_\pm = c^0_\pm e^{\mp\frac{e}{k_B T}(\psi(r,z)-\psi_0(z))}, \tag{7}$$

and therefore the local charge density can be written as

$$\rho_e eN_A(c^0_+ e^{-\phi} - c^0_- e^{\phi}), \tag{8}$$

where the dimensionless potential $\phi = \frac{e}{k_B T}(\psi - \psi_0)$ is introduced. The dimensionless potential describes the difference between an electric potential in the cylinder (r,z) and the potential on the central axis (0,z). After substituting this back in the Poisson equation, the Poison-Boltzmann equation for the dimensionless potential becomes

$$\nabla^2\phi = -\frac{e}{k_B T}\frac{e}{\varepsilon_0\varepsilon_r}N_A(c^0_+ e^{-\phi} - c^0_- e^{\phi}). \tag{9}$$

Another way to get to the Poisson-Boltzmann equation is by using Gibbs' variational principle for thermal equilibrium consisting of minimizing the system free energy, which will not be touched upon here. However it is interesting to look into [19]. In the next section a solution to the the Poison-Boltzmann equation for the dimensionless potential will be derived.

2.4.2 A Planar Wall Approximation

The dimensionless Poisson equation for the cylidrical system has been previously discussed. However, until now an analytical solution to this differential equation has not been found for the cylindrical case, which entails the Laplacian being $\nabla^2 = \frac{1}{r}\frac{d}{dr}(r\frac{d}{dr}) + \frac{d^2}{dz^2}$. Under the assumption that the induced electric field $E_r = -\nabla\phi_r$ in the radial direction as a result of the electric double layer is much larger than the induced electric field along the axis due to particle flow, $\frac{d^2}{dz^2}\phi \ll \frac{1}{r}\frac{d}{dr}(r\frac{d}{dr})\phi$, the derivative to the z component can be omitted. The notation ϕ_r refers to the potential for a arbitrary value of z. If this is combined with the assumption that the radius R of the channel is much larger than the Debye length, the Laplacian can be assumed to be $\frac{d^2}{dx^2}$, with $x = R - r$ as $\frac{1}{r}\frac{d}{dr}(r\frac{d}{dr}) = \frac{d^2}{dx^2} + \frac{1}{R-x}\frac{d}{dx}$. The final term can be ignored as a higher order term on the account of $R \gg x$ for the x close to the channel wall, where the electric double layer is. Under this assumption, the surface of the channel wall can be considered a planar wall instead of a cylindrical wall, with x being the distance to the wall. The Poisson-Boltzmann as a result of these specifications can be solved under the assumption that on the channel-axis both ion species have the same concentration $c^0(x = R, z) = c^0_+ = c^0_-$ as the dimensionless Poisson-Boltzmann is now given as

$$\frac{d^2}{dx^2}\phi = -\frac{e}{k_B T}\frac{e}{\varepsilon_0\varepsilon_r}N_A(c^0_+e^{-\phi} - c^0_-e^{\phi}) = N_A c^0\frac{e}{k_B T}\frac{e}{\varepsilon_0\varepsilon_r}(e^{\phi} - e^{-\phi}) = \kappa^2\sinh\phi, \tag{10}$$

with $\kappa(z) = \sqrt{2N_A c^0\frac{e}{k_B T}\frac{e}{\varepsilon_0\varepsilon_r}}$. This second-order partial differential equation can be solved under the following two boundary conditions. The first boundary condition is a symmetry condition $\frac{d\phi}{dx}|_{x=R} = 0$ and the second boundary condition is given by $\frac{d\phi}{dx}|_{x=0} = -\frac{e^2}{\varepsilon_0\varepsilon_r k_B T}\frac{\sigma_e}{e}$, which is a result of Gauss' law. These boundary conditions, combined with the use of a couple of mathematical identities and rewriting, give the unique solution to the second order derivative. The analytical non-linear solution for the dimensionless potential is given by

$$\phi(x, z) = 2\ln\frac{1 + \gamma e^{-\kappa(z)x}}{1 - \gamma e^{-\kappa(z)x}}, \tag{11}$$

with $\gamma = \frac{2\kappa}{G} - \sqrt{(\frac{2\kappa}{G})^2 + 1}$, $\kappa(z) = \sqrt{\frac{2c^0 N_A e^2}{k_B T\varepsilon_0\varepsilon_r}}$ and $G = -\frac{e^2}{\varepsilon_0\varepsilon_r k_B T}\frac{\sigma_e}{e}$. The explicit derivation of this solution can be found in appendix A. It is important to note that G is independent of axial position z and the only z dependent part of γ is κ. Using the fact that $x = R - r$ this can be substituted again to give the potential depending on r. This heterogeneous solution can be reduced to the homogeneous solution for the potential which is already known, under the condition that the Debye length is independent of the axial position and there is no concentration gradient [20, 21, 22, 23, 24].

2.5 The Fluid Velocity field

In the case of no external potential, which is ($\psi = 0$), the fluid flow as a result of a concentration gradient will be constant. This is shown by Equation 1 and 2. So the only way a concentration gradient can influence a fluid flow is due to an external potential. In this section the flow velocity field is derived using the Navier-Stokes Equation by treating the electric double layer as external potential.

2.5.1 The Navier-Stokes Equation

The stationary Navier-Stokes Equation for an incompressible fluid is given by

$$-\nabla p + \eta\nabla^2\mathbf{u} + \mathbf{F} = 0, \quad \nabla\cdot\mathbf{u} = 0, \tag{12}$$

with η the viscosity and p the pressure, under the assumption that the flow of the system is slow (this means a low Reynold's number). The flow velocity field $\mathbf{u} = \mathbf{u}(r, z)$ is divergence-free. The volume force is denoted

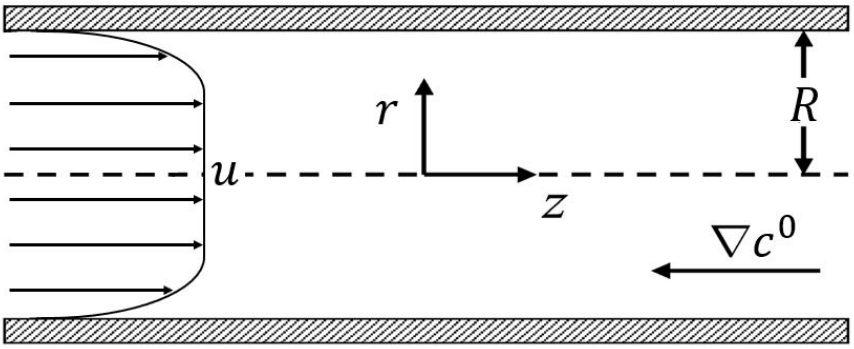

Figure 3: The fluid velocity u in the z direction of an nanochannel with radius R and concentration gradient ∇c^0. The dashed line represents the channel axis and the grey area the charged channel wall.

by $\mathbf{F}$, which describes the force on a volume element. If the electric double layer as a result of a charged channel surface is treated as an external potential, this volume force can be given as $\mathbf{F} = -eN_A(c_+ - c_-)\nabla\psi$. Substituting this in the Navier-Stokes equation gives

$$-\nabla p + \eta\nabla^2\mathbf{u} - eN_A(c_+ - c_-)\nabla\psi = 0,. \tag{13}$$

in the next section, the Navier-Stokes equation is used to first derive the induced pressure. Afterwards a solution for the fluid velocity field is derived.

2.5.2 The Axial Fluid Velocity

The only way a concentration gradient can induce a fluid flow, is through an external potential. For the system, this external potential is the electric double layer. However, a concentration gradient does not directly influence a fluid flow, which can also be seen in the Navier-Stokes equation (Eq. 13). The concentrations are given according to

$$c_\pm = c^0 e^{\mp\phi}. \tag{14}$$

In the infinite channel length case there is no fluid velocity in the radial direction. Under the assumption that the length L is much larger than the radius R, it is safe to assume that there is no fluid velocity in the radial direction for the finite length case as well. Figure 3 gives a overview of the situation. The radial component of the Navier-Stokes equation can then be written as

$$\frac{\partial}{\partial r}p = 2k_BTN_Ac^0\frac{\partial}{\partial r}\cosh\phi. \tag{15}$$

This gives the pressure as

$$p(r,z) = 2k_BTN_Ac^0(\cosh\phi - 1) + p_0. \tag{16}$$

Due to the fact that there can not be a fluid flow without external potential, the pressure outside the electric double layer must be constant. As there is no pressure difference between the two reservoirs, $p_0 = 0$. This pressure created by the concentration gradient induces a fluid flow. Substituting this back into the Navier-Stokes equation gives

$$-2k_BTN_A\frac{\partial}{\partial z}(c^0(\cosh\phi - 1)) + \eta\frac{\partial^2 u}{\partial r^2} + 2k_BTN_Ac^0\sinh\phi\frac{\partial\phi}{\partial z} = 0. \tag{17}$$

Using the fact that

$$\frac{\partial}{\partial z}(c^0(\cosh\phi - 1)) = \frac{\partial c^0}{\partial z}(\cosh\phi - 1) + c^0\sinh\phi\frac{\partial\phi}{\partial z}, \tag{18}$$

the partial differential equation of the fluid velocity can be written as

$$\frac{\partial^2 u}{\partial r^2} = 2\frac{k_BTN_A}{\eta}\frac{\partial c^0}{\partial z}(\cosh\phi - 1). \tag{19}$$

This second order derivative can be solved by using the substitution $x = R - r$ and the following two boundary conditions. The first boundary condition is that the fluid velocity constant is, $\frac{\partial u}{\partial r}|_{r=0} = 0$ The second boundary condition is the no-slip boundary condition at the channel wall. $u|_{r=R} = 0$. These boundary conditions, combined with the use of a couple of mathematical identities and rewriting, give an unique solution to the second order derivative. The analytical solution for the z component of the fluid velocity as a result of the concentration gradient is given by

$$u = \frac{-4k_BTN_A\kappa^{-2}}{\eta}\frac{\partial c^0}{\partial z}\ln\frac{1-\gamma^2e^{-2\kappa x}}{1-\gamma^2}, \tag{20}$$

with $\gamma = \frac{2\kappa}{G} - \sqrt{(\frac{2\kappa}{G})^2+1}$ and $\kappa = \sqrt{\frac{2c^0N_Ae^2}{k_BT\varepsilon_0\varepsilon_r}}$ and $G = -\frac{e^2}{\varepsilon_0\varepsilon_r k_BT}\frac{\sigma_e}{e}$. The explicit derivation of this solution can be found in appendix B. Using the fact that $x = R - r$ this can be substituted again to give the fluid velocity in the z direction depending on r,

$$u = \frac{-4k_BTN_A\kappa^{-2}}{\eta}\frac{\partial c^0}{\partial z}\ln\frac{1-\gamma^2e^{-2\kappa(R-r)}}{1-\gamma^2}. \tag{21}$$

2.6 The Debye length

The Debye screening length, which describes the thickness of the electric double layer is given by

$$\kappa^{-1} = \sqrt{\frac{k_BT\varepsilon_0\varepsilon_r}{2c^0N_Ae^2}}, \tag{22}$$

with c^0 in mM. Due to the fact that c^0 is not homogeneous on the channel axis, the Debye length is expected to change in the channel as well. As Reservoir 1 has a higher bulk concentration, the concentration of ions on the channel axis close to Reservoir 1 is higher than the concentration on the channel axis close to Reservoir 2. As according to the equation, the Debye length is inversely proportional to the concentration on the axis, it means that close to Reservoir 1 the Debye length will be smaller and the electric double layer will be thinner as compared to close to Reservoir 2.
At room temperature ($T = 298.15K$) and in water ($\varepsilon_r = 78.5$) [25], the Debye length is related to the concentration as

$$\kappa^{-1} = \frac{3.04}{\sqrt{c^0}} \quad \text{Å} \tag{23}$$

with c^0 now expressed in the unit M. As a result, for c^0 at 0.2, 0.5 and 1 M, the Debye length will be 6.8, 4.3 and 3.0 Å respectively. The Debye length κ^{-1} represents the distance it takes for the local potential to decrease to the e-th part of the potential at the surface, $\psi(\kappa^{-1}) = e^{-1}\psi(R)$ [26]. Therefore at three Debye lengths away from the electrode, the potential will have dropped to be a mere 0.6% of the original potential. For the three earlier named concentrations, three Debye lengths mean two or less nanometres.

2.7 Linear Response Theory

For small changes in the driving forces, the induced fluxes can be described by linear response theory. In this section the linear response theory will be discussed. It follows for the main part the discussion by Werkhoven [**?**]. In linear response theory, the relation between different driving forces (pressure, potential and concentration differences) and induced fluxes (volumetric flow rate Q, electric current I and salt flux J) as a result of these driving forces are quantified by a matrix M,

$$\begin{pmatrix} Q \\ I \\ J \end{pmatrix} = \frac{\pi R^2}{L} M \begin{pmatrix} \Delta p \\ \Delta\psi \\ \Delta\mu \end{pmatrix} \tag{24}$$

with M a symmetric 3×3 matrix and M_{ij} the transport coefficient. This matrix was first described by Onsager and is therefore called the Onsager matrix. These linear relation hold only for small changes in the driving forces (small Δp, $\Delta\psi$ and $\Delta\mu$). As the nanochannel of interest is a electric short-circuit channel,

this means that there is no potential dependent driving force ($\Delta\psi = 0$ over the channel), and is assumed to have a mechanical closed-circuit channel condition, no pressure dependent driving force ($\Delta p = 0$ over the channel), where the solvent can freely flow. It is however possible that the system has local pressure differences and potential differences. As a result, only the concentration gradient is non-zero. As a result volumetric flow rate Q, electric current I and salt flux J can be given as only a function of $\Delta\mu$, which is the chemical potential.
The chemical potential describes how species flow between different parts of a system. In an equilibrium state, the chemical potential of a species is uniform throughout the system and the net flow of particles is zero. If, however, there are heterogeneities of the chemical potential in the system, then particles will flow to decrease these overall differences in chemical potential. The chemical potential can be derived from the Gibbs free energy, which is given by

$$dG = -SdT + Vdp + \mu_+ dc_+ + \mu_- dc_-, \tag{25}$$

under the assumption that the temperature and the pressure are fixed in the two reservoirs, which is globally the case. This means that

$$\mu_\pm = (\frac{dG}{dc_\pm})_{T,p}. \tag{26}$$

The chemical potential is given by

$$\mu_\pm(0, z \to \infty) - \mu_\pm(0, z \to -\infty) = \Delta\mu = k_B T \ln \frac{c_{high}}{c_{low}}, \tag{27}$$

with c_{high} and c_{low} the concentration in the reservoirs.
The matrix elements which are globally relevant, can be understood by looking at the chemical potential and the induced fluxes. The matrix element M_{31}, M_{32} and M_{33} can be explicitly calculated for this system with a no slip boundary ($u(R, z) = 0$) on all the wall and equal mobility for both the cations and anions ($D_\pm = D$). The decision has been made to take the explicit formulas for these matrix elements out of the article made by Werkhoven instead of deriving them here [27].

2.7.1 The Volumetric Flux

The matrix element M_{31} describes the ratio between the concentration difference and the induced volumetric flux Q. In the case of an infinitely long channel, the volumetric flux can be given by

$$Q = \int dA u(r), \tag{28}$$

where $u(r)$ is the z-component of the velocity field. which entails the surface integral $\int dA = 2\pi \int_0^R dr r$ described by a plane with a fixed z cross sectioned with the channel. If the channel length is infinitely large, the velocity field is independent of translation on the z axis and there is no radial velocity. Under the assumption that the radius of the channel is far smaller than the length of the channel $R \ll L$ the formula for the volumetric flux can still be applied to the finite channel situation, as long as the cross section is far away enough from the channel entrances, so the influence of entrance effects will be rather small.
The explicit matrix element for the volumetric flux is given by

$$M_{13} = \frac{2e^2}{\eta\varepsilon_0\varepsilon_r k_B T}(2\ln\cosh\frac{1}{4}\phi_s - \frac{\kappa^2}{2R}\int_0^\infty ds(\cosh\phi(s) - 1)), \tag{29}$$

with $\phi_s = 2\ln\frac{1+\gamma}{1-\gamma}$ the potential at the channel surface and γ as defined in the solution of the dimensionless potential (Eq. 11) [27].

2.7.2 The Electric Current

The matrix element M_{32} describes the relation between the concentration difference and the induced electric current I. In the case of an infinitely long channel, the volumetric flux can be given by

$$I = e\int dA(j_+(r) - j_-(r)), \tag{30}$$

where $j_\pm$ denotes the z-component of the ionic flux $\mathbf{j}_\pm$ and the surface integral $\int dA = 2\pi \int_0^R drr$ as in the volumetric flux The explicit matrix element for the electric current is given by

$$M_{23} = -\frac{2D}{k_B T}\frac{\sigma_e}{z_s R} - \frac{2\varepsilon_0\varepsilon_r k_B T}{e\kappa^{-1}\eta R}\frac{z_s\varepsilon_0\varepsilon_r k_B T}{e^2}(4\frac{\sigma_e}{z_s e\sigma^*} - 2|\phi(R)|), \tag{31}$$

with $\sigma^* = 4\kappa^{-1}c^0 N_A$ and $z_s = \frac{\sigma_e}{|\sigma_e|}$ [27].

2.7.3 The Salt Flux

The matrix element M_{32} describes the relation between the concentration difference and the induced salt flux J.

$$J = \int dA(j_+(r) + j_-(r)), \tag{32}$$

with its components as defined in the section of the electric current. The explicit matrix element for the salt flux is given by

$$M_{33} = \frac{2Dc^0 N_A}{k_B T}(1 - 2\frac{\kappa^{-1}}{R}(2\sqrt{1 + (\frac{\sigma_e}{\sigma^* e})^2} - 2)) + \frac{4\varepsilon_0\varepsilon_r k_B T\kappa^{-1}c^0 N_A}{e^2\eta R}(4\sqrt{1 + (\frac{\sigma_e}{e\sigma^*})^2} - 4 - 16\ln\cosh\frac{\phi(R)}{4}). \tag{33}$$

[27]
The theoretical values resulting from these matrix elements will be compared to the numerical calculations of the full Poisson-Nernst-Planck-Stokes equation. In the next section discusses the numerical model used in the calculations.

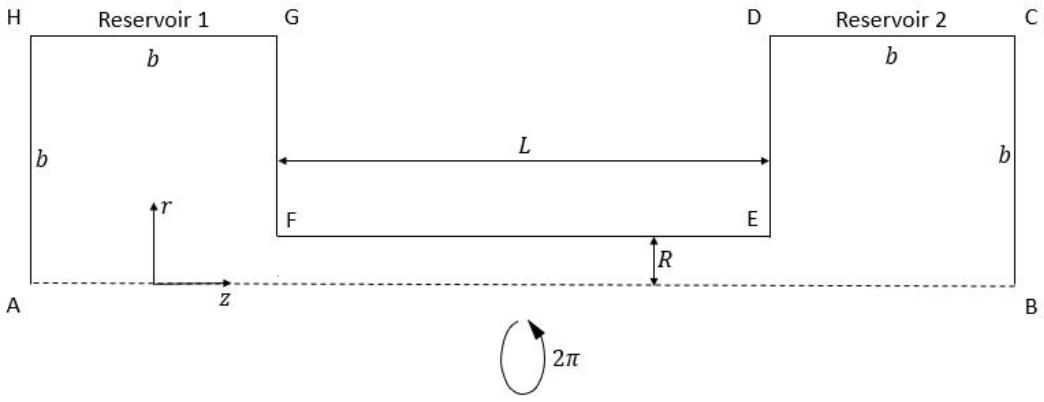

Figure 4: A schematic overview of the geometry. The dashed line AB represents the channel axis

3 Numerical Model

The theory derived in section 2 for the transport of fluids and charges in a nanochannel driven by a concentration gradient, can now be used to model the fluid and charge flow going through the nanochannel. To numerical model the equations discussed in the previous section a software called *COMSOL Multiphysics 5.4* is used. The *COMSOL Multiphysics* software uses a finite element method to run its calculations. The finite element method is used by computing the solutions to coupled partial differential equations like the Poisson-Nernst-Planck-Stokes equation and is quite powerful and versatile. The finite element method consists of subdividing a continuous domain into a set of finite elements, which are discrete sub-domains. As long as there is enough computing power, approximate solutions to the simulation can be found.[28][29] First the linear response relations described in the Onsager matrix M (Eq. 24) are considered to test the validity of the numerical model. This is to gain an insight into the parameter regimens for which the outlined theory holds.

3.1 The Geometry

The 3D system is modelled in *COMSOL Multiphysics* as a fully axis symmetrical geometry with axial coordinate z and radial coordinate r. The two reservoirs are built using two squares with length b, the nano channel consists of a rectangle with length L and height R.(Figure 4) The origin is placed in the middle of the channel and as a result $-L/2 \leq z \leq L/2$ and $0 \leq r \leq R$. The geometry is chosen in such a manner that the length L is much larger than the radius R and $b = L$ such that the reservoirs can be seen as large basins with a fluid volume and charge volume for which changes are so small compared to the changes in the channel that they can be neglected. The large enough basins ensure that all the variables decay to their bulk value. To ensure that non-overlapping electric double layers are considered, the maximum placed on the possible Debye lengths as a result of the concentration gradient consists of the Debye length being at least a factor 5 smaller that the channel radius R, in the case of the radius being 5 nm, this means that the concentration in the channel everywhere along the axis need to be at least 90 mM (Eq. 23).
The Electrostatics, Transport of Diluted Species and Laminar Flow interfaces of COMSOL Multiphysics were employed to couple the Poisson-Boltzmann (Eq. 3), Nernst-Planck (Eq. 1) and Navier-Stokes (Eq. 13) equation, respectively.

3.2 The Boundary Conditions

To solve the differential equations describing the electrokinetic flow discussed in the theory, different physics modules need to be implemented in *COMSOL Multiphysics*. The electric double layer can be modelled using the *Electrostatics* module in *COMSOL Multiphysics* by adding a surface density σ_e to the surface on the channel. The particle flow can be solved using the the *Transport of Diluted Species* module in *COMSOL Multiphysics* and the fluid flow can be solved using the the *Creeping Flow* module in *COMSOL Multiphysics*.

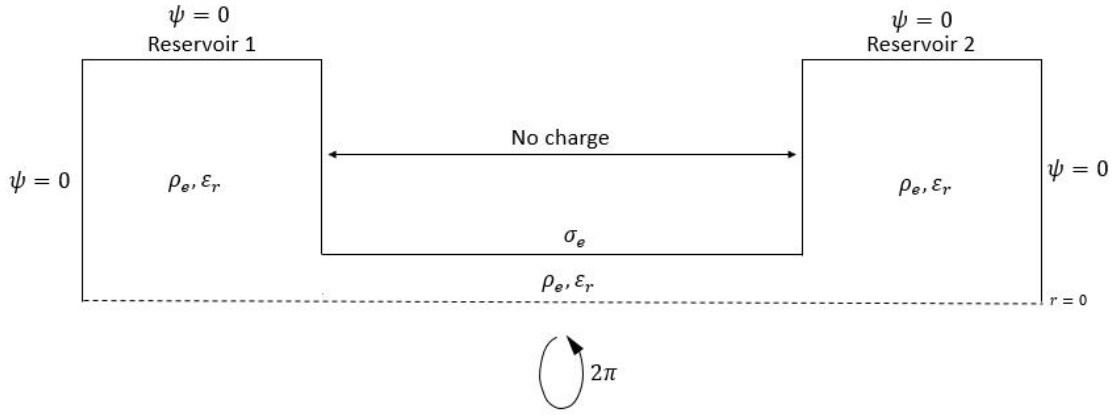

Figure 5: The boundary conditions for the Poisson equation. The channel side walls carry no charge density (hence $\mathbf{n} \cdot \nabla\psi = 0$), and the channel carries a charge density σ_e. The fluid in the interior has a relative permittivity of ε_r and has local charge density ρ_e. The boundaries representing the reservoir interior are grounded ($\psi = 0$).

For all three modules, special boundary conditions need to be implemented and the modules are coupled by the local charge and volume force.

3.2.1 The Poisson Equation

The *Electrostatics* interface in *COMSOL Multiphysics* is used to calculate the electrostatic potential in the system. The space charge density ρ_e defined on the entire domain is given by $eN_A(c_+ - c_-)$ $[C/m^3]$ as described in the theory (the ion concentrations with valency 1 and -1 respectively). The relative permittivity of the solvent ε_r is specified as it being that of water $\varepsilon_r = 78.5$. The channel wall EF has a surface charge density given by $\sigma_e = 1/100$ $[e/nm^2]$ (with e the elementary charge) which is a constant homogeneous across the channel wall. On the reservoir walls FG and DE the boundary condition of $\mathbf{n}\cdot\nabla\psi$ is specified by using the *Zero Charge* module. A ground condition consisting of the electric potential ψ being set zero is specified on channel walls AH, GH, BC and CD (so $\Delta\psi$). (Figure 4) A schematic overview of these boundary conditions can be found in Figure 5.

3.2.2 The Nernst-Planck Equation

The *Transport of Diluted Species* interface in *COMSOL Multiphysics* is used to calculate the movement of the ions in the solution. The transport mechanisms of conviction and diffusion in an electric field are included in the Nernst-Planck equation and the existence of the two ion species c_+ and c_- are specified. The potential ψ determined by the electrostatics interface and the fluid velocity u determined by the laminar flow interface are used as input combined with the temperature $T = 298.15K$, diffusion coefficient $D_\pm = 10^{-9}$ $[m^2/s]$ and the corresponding valency of the species. On the boundaries DE, EF and FE (Figure 4) a no-flux ($-\mathbf{n} \cdot (\mathbf{J}_\pm + \mathbf{u}c_\pm) = 0$) boundary condition is applied, on boundaries BC and CD representing the interior of reservoir 2, the concentration constraint $c_\pm = c_{low}$ is specified,on boundaries AH and GH a concentration constraint of $c_\pm = c_{high} = ac_{low}$ is specified with c_{high} and c_{low} constant values in the system. The variable $a = \frac{c_{high}}{c_{low}}$ describes the change in concentration between the two reservoirs. A schematic overview of the relevant boundary conditions is presented in Figure 6.

3.2.3 The Navier-Stokes Equation

The *Laminar Flow* interface in *COMSOL Multiphysics* is used to calculate the velocity field $\mathbf{u}$ $[m/s]$ and local pressure p $[Pa]$. The flow is set to incompressible flow with neglecting the inertial term and non-turbulent. The fluid is given the density ρ $[kg/m^3]$ and dynamic viscosity η $[Pa \cdot s]$. A volume force is defined by

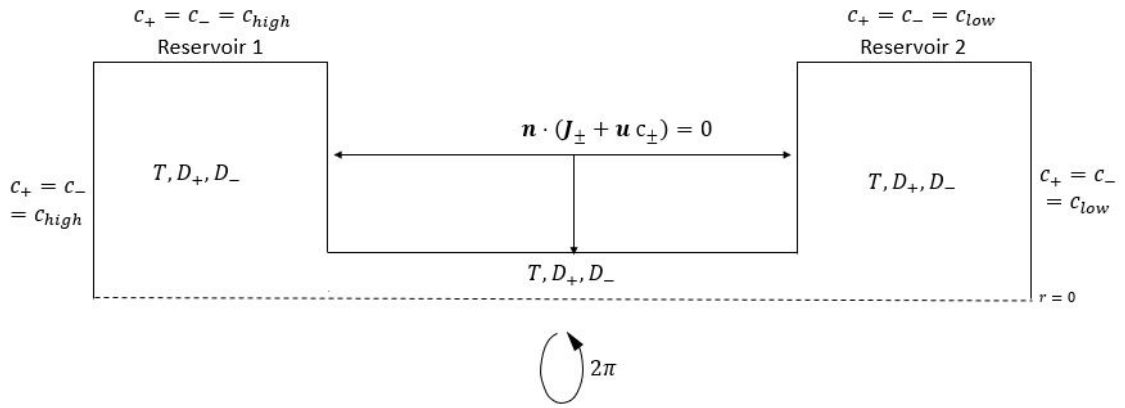

Figure 6: The boundary conditions for the Nernst-Planck equation. The channel side walls and channel wall have no flux ($\mathbf{n} \cdot (\mathbf{J}_\pm + \mathbf{u}c_\pm) = 0$) going through them. The fluid in the interior has a temperature T and diffusion coefficient D_+ and D_- for respectively the cation and anion species. The boundaries of the interior of reservoir 1 have for both species the same c_{high} concentration constraint and the boundaries of the interior of reservoir 2 have for both species the same c_{low} concentration constraint.

$\mathbf{F} = -eN_A(z_1c_+ + z_2c_-)\nabla\phi$ with e the elementary charge and N_A the number of Avogadro as in the theory. The fluid velocity on the channel wall and side walls is set to zero. An inlet on the interior walls of reservoir 1 is defined by pressure constraint $p = 0$ and an outlet on the interior walls of reservoir 2 is defined by pressure constraint $p = 0$, so $\Delta p = 0$. A schematic overview can be found in Figure 7.

3.3 The Mesh

To apply the finite element method, it is necessary for an appropriate mesh to be created for the system. The mesh is used to discretize the areas in which the differential equation describing the system needs to be solved. On the corners of the triangular and quadrangular elements of the mesh, the desired physical values are given. Once there are enough of these evaluation point, the solutions given by this numerical approach will closely resemble to the analytical solutions of the theory. This means that if the mesh is too coarse, the finite element method will fail to find a suitable approximate solution. On the other hand, when the mesh is too fine, the program will use a long time and significant computing power to find a solution. In the best case scenario, the mesh is just fine enough to arrive at a suitable solution. As it is expected that the solution changes a lot in the electric double layer, a denser mesh needs to be made close to the channel wall. As long as the solutions found numerically appear to be continuous, there is no need for a denser mesh, however if discontinuities appear in these solutions, the mesh should be reconsidered.
The system will be divided in a couple of domains. One sub-domain consist of a box with region $3R/4 \leq r \leq R, -L/2 \leq z \leq L/2$ near the channel wall. The mesh in this domain is a structured quadrilateral mesh with its maximum element size set to $R/40$ Another sub-domain consists of two small boxes around the middle of the channel ($-R/2 \leq z \leq R/2$), with in which the squared box ($3R/4 \leq r \leq R$) close to the charged wall has a mesh mapped with maximum element $R/80$. The rest of this sub-domain ($0 \leq r \leq 3R/4$) has a mapped mesh with maximum element size $R/40$. The reason for this domain is to check the linear response theory at $z = 0$ (in the middle of the channel length). Another sub-domain consists of the rest of the channel and two quarter circles at the end of the channel with radius $2R$, in here the mesh is created by covering the entire sub-domain in triangular elements with maximum element size set to $R/5$. The rest of the domain is filled with a triangular mesh with maximum element size set to $R/2$. The rest of the settings in the meshes are predefined. An schematic view of all the meshes can be found in Figure 8.

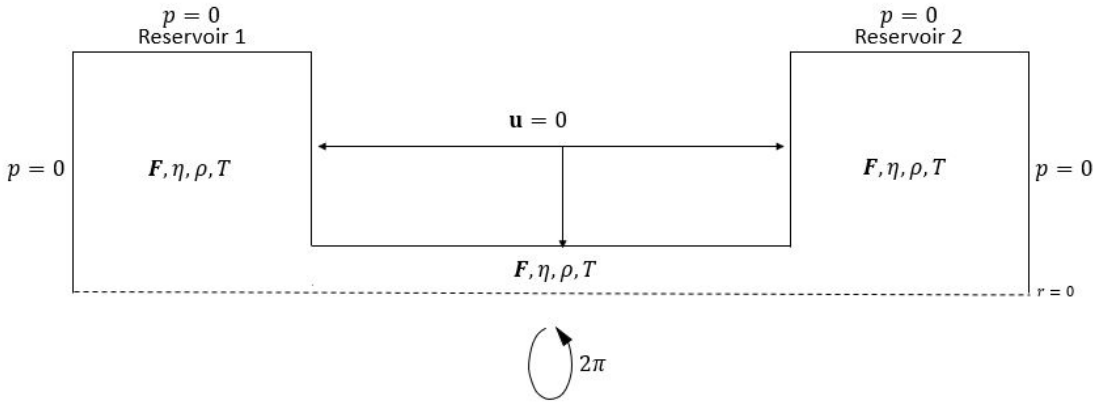

Figure 7: The boundary conditions for the Navier-Stokes equation. The channel side walls and the channel have a fluid velocity constraint of $\mathbf{u} = 0$. The fluid in the interior has a density of ρ, volume force $\mathbf{F} = -eN_A(z_1c_+ + z_2c_-)\nabla\phi$, temperature T and dynamic viscosity μ. The boundaries representing the reservoir interior have a no pressure constraint ($p = 0$).

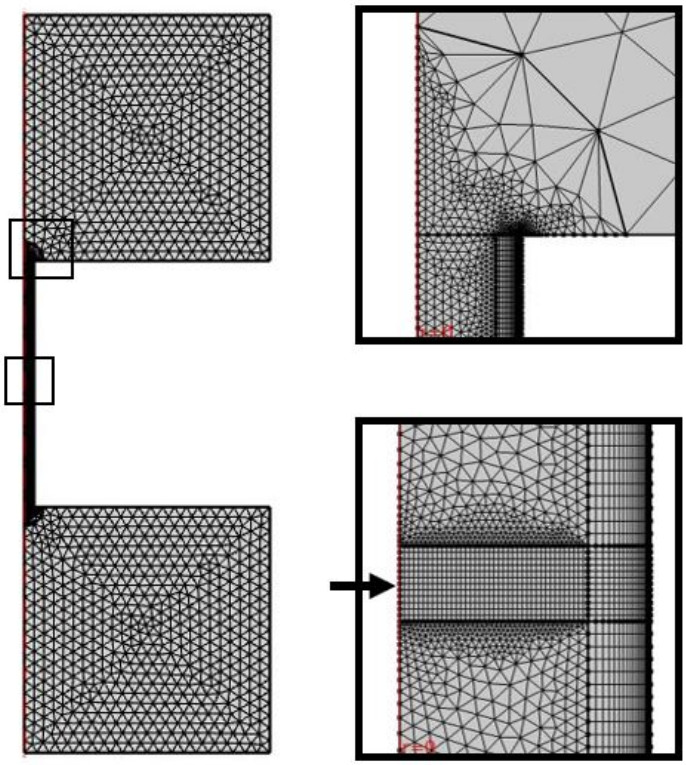

Figure 8: A screen shot of the entire mesh build in the geometry and close ups of the areas of interest, all three of them generated by COMSOL Multiphysics. The radius is set to $R = 50$nm and the channel length is set to $L = 1500$nm. The squares of the reservoir are set to have the same length L. The two boxes in the close up of the middle of the channel (lower right) have both a hight of $R/4$ and a width of respectively $3R/4$ and $R/4$ viewed left to right. The arrow is pointing at $z = 0$. In the close up of a entrance of the channel (upper right) the more densely packed area represents the mapped mesh close to the charged wall.

Quantity	Symbol	Value	Unit
Surface charge density	σ_e	$1 \cdot 10^{-}2$	e/nm
Diffusion coefficient	$D = D_+ = D_-$	$1 \cdot 10^{-}9$	m^2/s
Charge valency	$z_+ = -z_-$	1	1
Dynamic viscosity	η	$8.925 \cdot 10^{-4}$	pa·s
Mass density solvent	ρ	Value	Unit
Temperature	T	298.15	K
Relative permittivity	ε_r	78.5	1
Channel radius	R	50	nm
Channel length	L	1500	nm
Ionic concentration lower boundary	c_{low}	1	mM
Ionic concentration higher boundary	$c_{high} = a \cdot c_{low}$	1	mM
Fraction of concentration change	$a = c_{high}/c_{low}$	1	1

Table 1: For the simulation of the nanochannel, relevant parameter values of water are used in *COMSOL Multiphysics*. Parameters used in COMSOL to simulate the linear response behaviour for small concentration differences.

4 Results

In this section will first consider the linear response relation between the chemical driving force as a result of a concentration gradient and the induced fluxes by this concentration gradient, consisting of the fluid volume flux Q, the electric current I and the salt flux J. After this, the analytical expressions found for the potential and the fluid velocity field will be compared to the numerical results given by *COMSOL Multiphysics*.

4.1 Linear Response

In Figure 9 the linear response regime of the volumetric flux, the electric current and the salt flux for both the lower boundary concentration in the reservoir $c_{low} = 1$mM and $c_{low} = 5$mM are plotted against the fraction on concentration change parameter which describes the chemical potential gradient. The linear relations plotted are a result of applying Equation 29, 31 and 33. Unfortunately, some of the linear response relations are not fully reproduced, this is most likely due to small calculation errors in the computation of the theoretical values, which have not been found yet. The fact that the linear response relations are not fully reproduced does not mean that the data which is given by *COMSOL Multiphysics* should be interpreted as being false. *COMSOL Multiphysics* solving the coupled Poisson-Boltzmann, Nernst-Planck and Navier-Stokes equations to derive the induced fluxes and the linear response relations are derived from these same equations. As it is known that the coupled Poisson-Boltzmann, Nernst-Planck and Navier-Stokes equations are correct, the results given in *COMSOL Multiphysics*, which are an immediate result of solving these equations, should not have to be interpreted as being false. Despite good efforts, these numerically solutions to these coupled equations are not fully derived theoretically.
In Figure 10 the induced volumetric flux, electric current and salt flux for both the lower boundary concentration in the reservoir $c_{low} = 1$mM and $c_{low} = 5$mM are plotted against the fraction on concentration change parameter which describes the chemical potential gradient. The linear relations plotted are fitted over the first data points at low salt concentration gradients, from $a = c_{high}/c_{low} = 1.00001$ to $a = c_{high}/c_{low} = 1.01$. It can be seen that the relation between the volumetric flux and the chemical potential gradient can not be described by the linear relation theory for $a = c_{high}/c_{low} = 1.5$. for both lower boundary concentration $c_{low} = 1$mM and $c_{low} = 5$mM. When investigating the potential and the fluid velocity field, it should be kept in mind that the linear response region is in this range. It can be seen that the volumetric flux for a lower boundary concentration of $c_{low} = 5$mM has a slope in the linear response regime of approximately 5 times as high as the slope of the volumetric flux for a lower boundary concentration of $c_{low} = 1$mM.
The slope of the electric current in the linear response regime is almost the same for both lower boundary

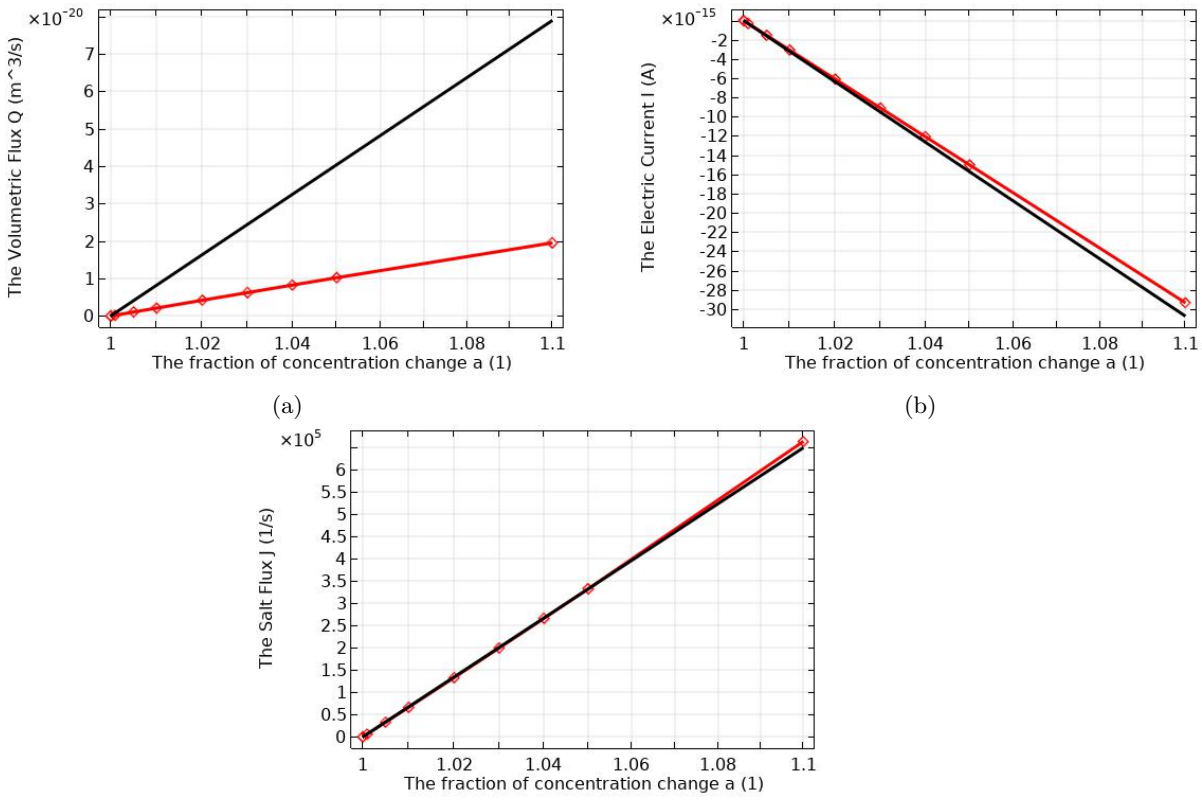

Figure 9: The induced volumetric flux (a), electric current (b) and salt flux (c) from the imposed concentration gradient on the nanochannel model in *COMSOL Multiphysics* for the fraction of change $a = 1.00001, 1.0001, 1.001, 1.0005, 1.01, 1.02, 1.03, 1.04, 1.05, 1.1$ for the lower reservoir concentration $c_{low} = 1\text{mM}$ (Red). The other line denotes the analytical value resulting form the linear response theory for $c_{low} = 1\text{mM}$ (Black) according to Equation 29, 31 and 33.

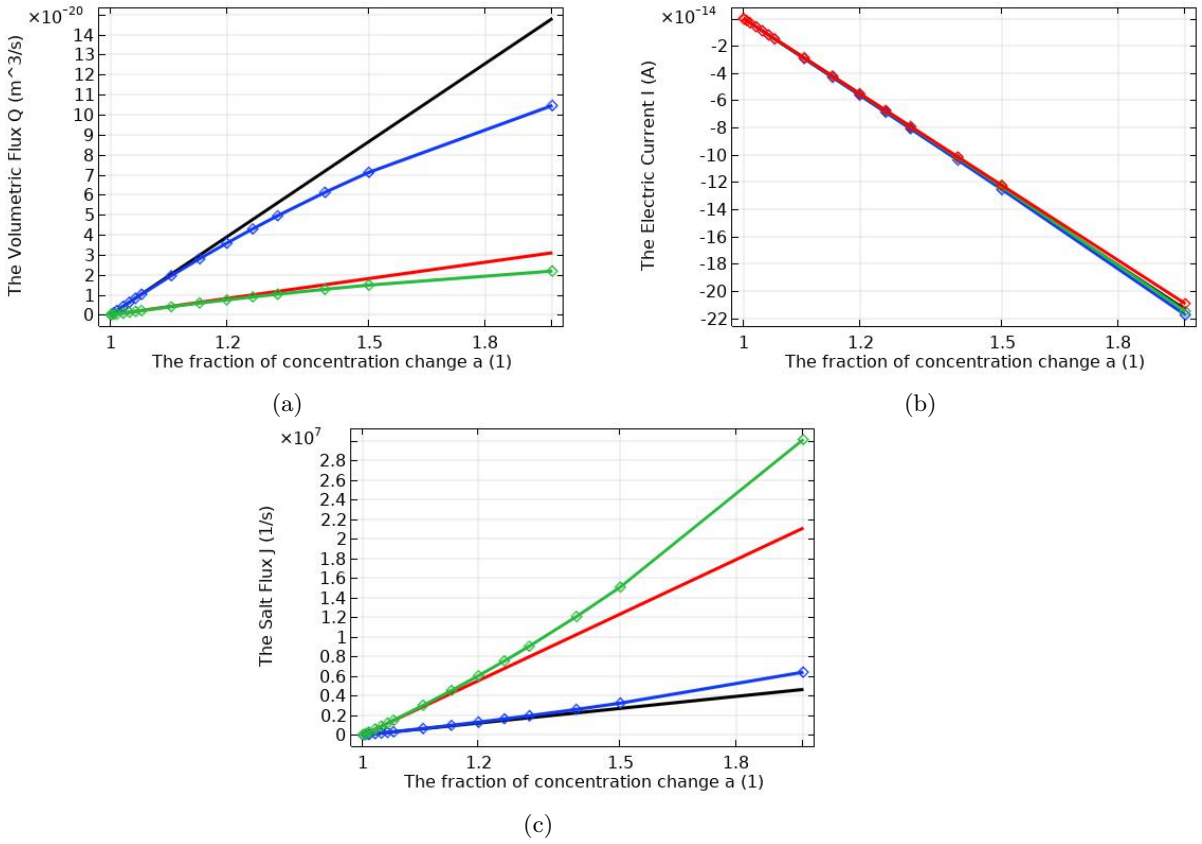

Figure 10: The induced volumetric flux (a), electric current (b) and salt flux (c) from the imposed concentration gradient on the nanochannel model in *COMSOL Multiphysics* for the fraction of change $a = 1.0001, 1.001, 1.01, 1.02, 1.03, 1.04, 1.05, 1.1, 1.15, 1.2, 1.3, 1.5$ and 2 for both the lower reservoir concentration $c_{low} = 1$mM (Blue) and $c_{low} = 5$mM (Green). The two straight lines denote fitted linear relations for $c_{low} = 1$mM (Black) and $c_{low} = 5$mM (Red).

concentration $c_{low} = 1$mM and $c_{low} = 5$mM. The electric current for both concentration $c_{low} = 1$mM and $c_{low} = 5mM$ fails to follow the linear response relation after approximately $a = c_{high}/c_{low} = 1.5$.
It can be seen that the salt flux for a lower boundary concentration of $c_{low} = 5$mM has a slope in the linear response regime of approximately 4.5 times as high as the slope of the salt flux for a lower boundary concentration of $c_{low} = 1$mM. The salt flux for both concentration $c_{low} = 1$mM and $c_{low} = 5$mM fails to follow the linear response relation after approximately $a = c_{high}/c_{low} = 1.2$.
Unfortunately the analytical solutions to the linear response relations have not been plotted against the data given by *COMSOL Multiphysics* in Figure 10. The calculation of the matrix elements M_{31}, M_{32} and M_{33} from the Onsager matrix are lengthy and therefore have a lot of room for errors. For now, the analytical results do not match the numerical results perfectly. However, the regime for which the nanochannel can be described with the linear response relations, has been found.

4.1.1 The Potential

In this section the analytical derived expression for the potential inside the nanochannel and the numerical solutions for the potential generated by *COMSOL Multiphysics* will be compared.
In Figure 11 the numerical solutions for the electric potential, corrected with $\frac{e}{k_B T}$ to make its unit dimensionless, are plotted for different z-planes in the channel along with the expected electric potential according to the analytical expression derived in the theory section. The situation for which these numerical solutions are found, can be described by the lower boundary constraint $c_{low} = 1$mM, fraction of change $a = 2$ and the rest of the parameters of this situation are given in Table 1. As was seen in the linear response section, $a = 2$

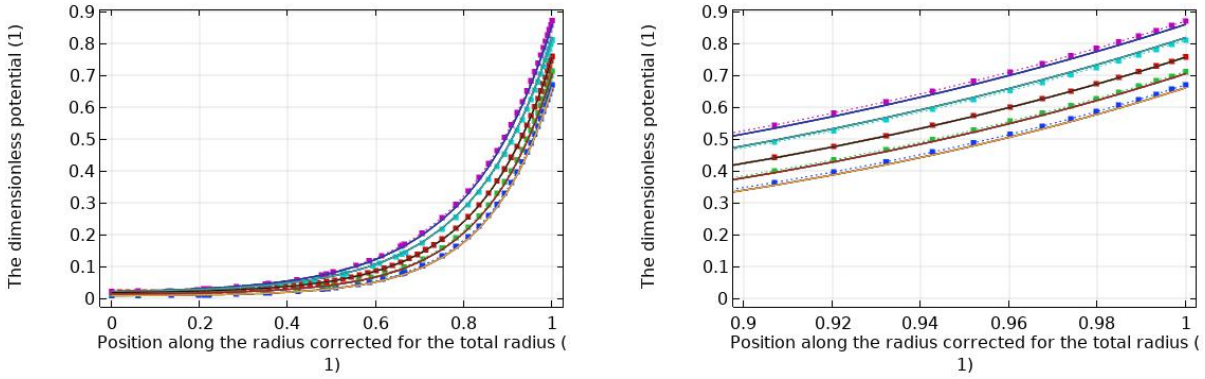

(a) (b)

Figure 11: The electric potential for the situation defined by the lower boundary condition $c_{low} = 1\text{mM}$ and fraction of concentration change $a = c_{high}/c_{low} = 2$. The dimensionless potential, $\frac{e}{k_B T}\psi$, is viewed at different z-planes, $z = -4L/10$ (Purple), $-2L/10$ (Light Blue), 0 (Red), $2L/10$ (Green) and $4L/10$ (Blue) along the channel radius, which is given as r/R. The analytical solutions for this dimensionless potential $\phi + \frac{e}{k_B T}\psi_0$ are given for these different z-planes as well. An overview is given in (a) and and (b) gives a close up of the potential in the electric double layer.

does not fall into the linear response regime. However, the analytical expression for the potential derived in the theory section is a non-linear solution. It can indeed be seen that this non-linear solution describes the situation properly, as the analytical solution fits the numerical solution almost perfectly. The reason why it is almost perfectly and not perfectly can be motivated by errors occurring due to for example entrance effects. This raises a new question. Is there a point were these errors are too large to ignore and the analytical expression found in the theory section does not describe the numerical situation properly. In other words, when are the assumptions which where made to derive this analytical expression no longer valid. *COMSOL Multiphysics* generates the numerical solution by solving the coupled Poisson-Boltzmann, Nernst-Planck and Navier-Stokes equations and the analytical solution is derived in the theory by the use of these same equations in combination with a couple assumptions of the situation. It is therefore more likely that at one point the analytical solution no longer describes the situation than that the data generated by *COMSOL Multiphysics* is faulty, as the numerical solution does match the theory for the situation described above.
In Figure 12 the numerical solutions for the electric potential, corrected with $\frac{e}{k_B T}$ to make its unit dimensionless, in the middle of the channel ($z = 0$), are plotted for different fractions of change ranging from $a = 1.1$ to $a = 30$ along with the expected electric potential according to the analytical expression derived in the theory section for these fractions of change. It can be seen that even though these fractions of change fall far outside the linear response regime, the numerical solutions and the analytical solutions for the electric potential match each other quite well if errors are taken into account due to entrance effects. As the analytical expression found in the theory is a non-linear solution, it is expected to match the numerical solution outside the linear regime as well. As Figure 12 show that even for a large concentration gradient like fraction of change $a = 30$ the analytical solution is a good fit to the numerical solution, the analytical solution found in the theory can indeed be used to describe the electric potential inside the charged nanochannel under the condition that the electric potential and the concentration on the channel axis is known.
The analytical expression for the electric potential is a good fit to the numerical solutions found by *COMSOL* for fractions of change $a = 30$ and smaller. It is possible that even for larger fractions of change, this is still the case. In the next section the expression derived in the theory for the z-component of the fluid velocity field will be compared to the numerical solutions generated by *COMSOL*.

4.1.2 The Velocity

In this section the fluid velocity field will be discussed. First the analytical derived expression for the fluid velocity in the z direction inside the nanochannel and the numerical solutions for this fluid velocity component generated by *COMSOL Multiphysics* will be compared. Afterwards the fluid velocity field for a

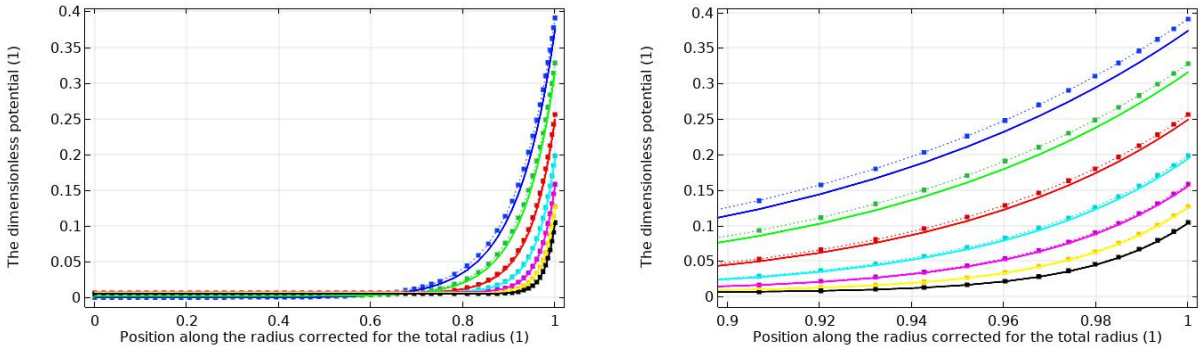

(a) (b)

Figure 12: The electric potential for the situation defined by the lower boundary condition $c_{low} = 5\text{mM}$ in the middle of the channel, z-plane $z = 0$. The numerical solutions for the dimensionless electric potential, $\frac{e}{k_B T}\psi$, are viewed for different fractions of change $a = 1.1$ (Blue), $a = 2$ (Green), $a = 4$ (Red), $a = 7.5$ (Light Blue), $a = 12.5$ (Purple), $a = 20$ (Yellow) and $a = 30$ (Black). The analytical solutions for this dimensionless potential $\phi + \frac{e}{k_B T}\psi_0$ for these different fractions of change are given as well in as solid lines in the same colour. An overview is given in (a) and and (b) gives a close up of the potential in the electric double layer.

small concentration gradient (low value for the fraction of change) will be compared to a large concentration gradient (high value for the fraction of change.)

In Figure 13a the numerical solutions for the situations described by low concentration boundary $c_{low} = 5\text{mM}$ and fractions of change $a = 1.005$, $a = 1.01$, $a = 1.02$, $a = 1.03$, $a = 1.04$ and $a = 1.05$. These solutions for the z-component of the velocity field,given by *COMSOL Multiphysics*, are plotted. These solutions are viewed at the middle of the channel, z-plane $z = 0$, along the channel radius, which is given as r/R. Together with these numerical values, the analytical solutions found for the fluid velocity in the z-direction is plotted. It can be seen that even though the analytical solutions come close to the numerical solutions, they do not completely match. As all fractions of change are chosen inside the linear response regime, this is against expectations. There could be several reasons behind this discrepancy between the numerical and analytical solutions. First of all, to calculate the analytical solution, values for the concentration gradient on the channel axis were requested in *COMSOL Multiphysics* with the use of *Point Evaluation*. This might be the reason behind the discrepancy happening on 4/5-th of the radius. If the values at the channel axis given by *COMSOL Multiphysics* are a bit lower than that they should be with the assumption of a constant velocity field outside the electric double layer and corrections for this are made, the analytical solutions would fit the numerical solutions in the electric double layer region better. However if that is the case, the lowering of the value at the channel axis indicates that there is a small back-flow occurring.

A close up of the velocity vector field at $z = 0$ for $a = 1.05$ generated by *COMSOL Multiphysics* is given in Figure 13c. It can be seen that the velocity outside the electric double layer region is decreasing. This is against expectations, as without an external potential the concentration gradient can't induce a fluid flow. The fact that there is a decrease in velocity means that there needs to be an external potential which is not the electric double layer as well.

Figure 13b shows the numerical solutions for the z-component of the velocity field at the middle of the channel, z-plane $z = 0$, along the channel radius, given as r/R, for different fractions of change with lower boundary concentration $c_{low} = 5\text{mM}$. These fractions of change range from $a = 1.1$ to $a = 30$. It can be seen that the shape of the solutions changes as the fractions of change are a higher value. For low fractions of change, the shape of the graph is almost constant outside of the electric double layer and decreases to zero with an arch in the electric double layer region. For high fractions of change, the graph still decreases to zero inside the electric double layer (as expected due to the no-slip boundary condition on the channel wall), however outside the electric double layer, the shape is not a constant line any more but appears to be a parabolic shape.

As the shape outside the electric double layer for high fractions of change appears to be of the same shape which would result from an electrical ($\Delta psi \neq 0$) driving force (electric-osmosis) [9]. This would mean that

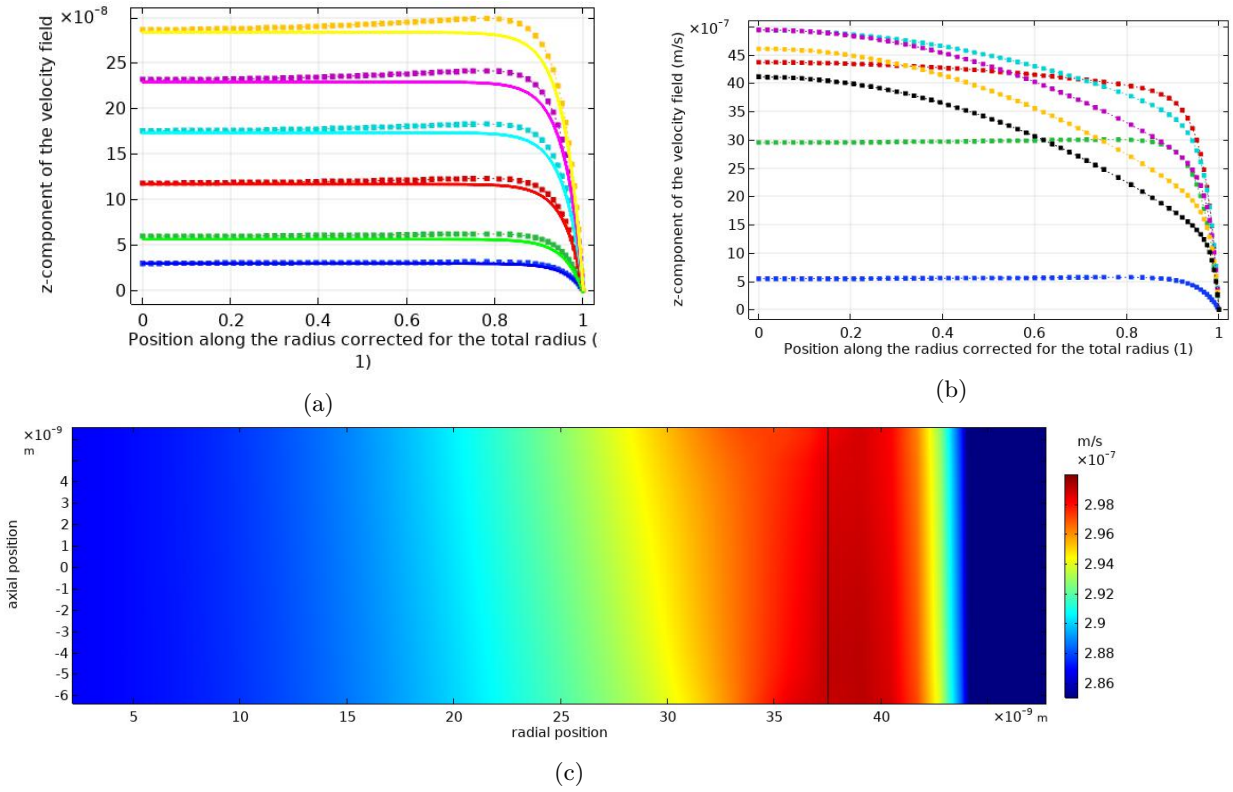

Figure 13: The z-components of the velocity field at $z = 0$ for fractions of change $a = 1.005$ (Blue), $a = 1.01$ (Green), $a = 1.02$ (Red), $a = 1.03$ (Light Blue), $a = 1.04$ (Purple) and $a = 1.05$ (Yellow) are plotted against the position along the radius r/R.(a) The analytical solutions for these z-components are plotted in the same colour as the numerical date. In Figure (b) the numerical solutions for the z-component of the velocity field are plotted at $z = 0$ for fractions of change $a = 1.1$ (Blue), $a = 2$ (Green), $a = 4$ (Red), $a = 7.5$ (Light Blue), $a = 12.5$ (Purple), $a = 20$ (Yellow) and $a = 30$ (Black). In (c) the velocity field for the fraction of change $a = 1.05$ is given as a 2D-plot, with horizontally the radial position r and vertically the axial position z.

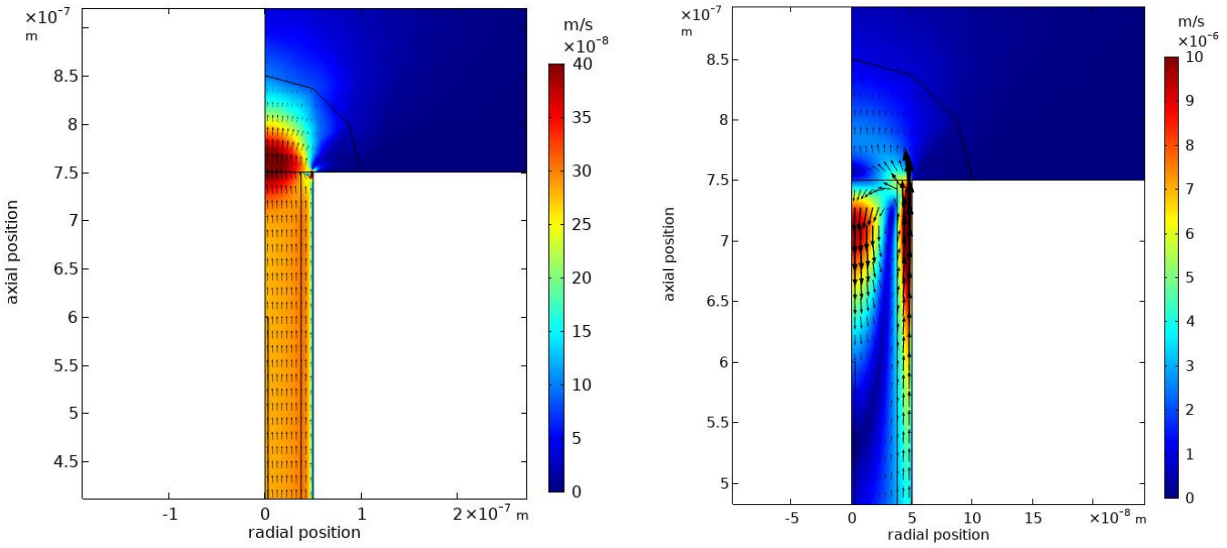

(a) (b)

Figure 14: The velocity fields for the fraction of change $a = 1.05$ (a) and $a = 30$ (b) for lower boundary concentration $c_{low} = 5$mM are given as a 2D-plot, with horizontally the radial position r and vertically the axial position z. The legends explaining the magnitude of the velocity are given at the right of each plot. The black arrows are used to denote the direction and strength of the vector field.

the fluid flow going in the radial direction at the entrance induces an potential drop over the channel and the assumption of only a chemical driving force would be invalid.
In Figure 13b can also be seen that the value of the z-component of the velocity on the channel axis will rise if the fraction of change gets higher for fractions of change $a = 1.1$ to $a = 4$. At $a = 7.5$ the z-component seems to have reached its maximum value and after this will decrease. This behaviour of the z-component for high fractions of change is not expected according to the analytical solution derived in the theory.
The reason why there is a discrepancy between the analytical and numerical solutions has to originate from the assumptions made to derive the analytical expression for the z-component of the velocity field. One of the assumptions made was that there is no fluid velocity in the radial direction as this was true for an infinite channel length. However at the entrance of the low concentration reservoir, there is a fluid velocity in the radial direction as the channel stops. For small changes in concentration gradient, these entrance effects are playing less of a role than for large changes in concentration gradient. This would explain the interesting behaviour shown in Figure 13b.
In Figure 14 the velocity field at the lower concentration reservoir ($c_{low} = 5$mM) is plotted for fractions of change $a = 1.05$, which falls into the linear response regime, and $a = 30$ where the entrance effects are expected to play a mayor role according to the earlier reasoning. It can indeed be seen that there is a difference in behaviour of the vector field for these two situations. For the fraction of change inside the linear response regime, the region inside the channel outside the electric double layer appears to be mostly uniform. There is a bit of entrance effects going on, but their influence to the vector field inside the channel is small. For the fraction of change far outside the linear response regime the entrance effects result in a flow back into the channel. Under the reasoning that the entrance effects result in an electric field over the channel, this back flow can be explained. However this back flow at the entrance was not predicted by the analytical expression derived in the theory section.

5 Discussion

This discussion will primarily focus on changes in the potential and fluid velocity field depending on the concentration gradient since the linear response relations are expected outcomes and will therefore not lead to new insights regarding the research questions outlined in the introduction. Even though the linear response theory has not exactly verified the simulations of the model build with *COMSOL Multiphysics*, it is only a matter of thoroughly going over the calculations until its validity is assured. This is not the case at the moment and since the Onsager matrix from the linear response theory should verify the considered nanochannel systems up to errors coming from the entrance effects. The results of the linear response theory for the different induced fluxes are to be used as indication of the valid regimes for which in principle analytical solutions for the potential and fluid velocity field can be found.

The results given in the previous section show that the analytical expression derived to describe the electric potential of the electric double layer inside the channel match the numerical results generated by *COMSOL Multiphysics*. However it has to be noted that to get the Debye length, the concentration of the ionic species is gained with *Point Evaluation* from *COMSOL Multiphysics* as was done for the electric potential on the channel axis to get the full analytical expression. This implies that the analytical expression describes the system quite well, provided that the values taken in from the channel axis are valid. This may also explain the fact that the analytical expression matches the numerical solutions generated by *COMSOL Multiphysics* far outside the linear response regime, as data points were taken from these numerical solutions. It therefore raises the question of what the regime in which applicability of this analytical expression would be valid if the potential along the axis was described in an analytical manner.

The most interesting results of those who will be discussed, are the results of the fluid velocity field for different concentration gradients. The results show that inside the linear response regime, the analytical expression for the z-component matches the numerical solutions generated by *COMSOL Multiphysics* fairly well. There is however a small decrease in velocity outside the electric double layer region. This behaviour can be motivated by entrance effects. It is however important to note that *Point Evaluation* was used again to get the necessary values of the parameters on the channel axis for the analytical expression.

Far outside the linear response regime, with fraction of change $a = c_{high}/c_{low} \geq 4$, the entrance effect have a large influence on the fluid vector field of the system and the analytical and numerical solution do not match. The most likely cause for this discrepancy in the z-component of the velocity field to happen, would be the fact that at the channel entrance, the assumption that there is no fluid flow in the radial direction is no longer valid. This fluid flow may give rise to a difference in potential over the channel, which will be a driving force as well. If there is a bigger difference in concentration between the two reservoirs, the fluid flow in the radial direction will be larger as well. This means that the driving force as a result of this fluid flow has a greater influence on the fluid flow in the channel. This may be a reason behind the parabolic shape found in the results for the z-component of the velocity.

As the analytical expression does not take this back flow as a result of entrance effects into account, it does not properly describe the situation in the nanochannel. However, for small concentration differences it can still be used to get an estimation of the behaviour inside the channel.

6 Conclusion

A nanochannel subjected to a concentration gradient in a system described by the concentration boundaries $c_{high} > c_{low}$ and the rest of the parameters as described in Table 1 will generate a volumetric flux, electric current and salt flux. These induced fluxes are linear with respect to the chemical driving force at least until $c_{high}/c_{low} = 1.1$. For smaller concentration differences then this, the induced fluxes can be described by Onsager's linear response theory.
The dimensionless potential derived in the theory section which takes the axial dependent Debye length into account, can be used to describe the electric potential of the discussed system and the heterogeneities of the electric double layer in the nanochannel. This answers the research question raised in the introduction. It is indeed possible to describe the heterogeneous electric double layer for this system in an analytical manner. The same can't be said for the fluid velocity field. It appears that the complete behaviour of the fluid velocity field in the system can not be completely described in an analytical manner as of now. However, for special situations the behaviour can be predicted.
Leaving as a conclusion is that the velocity field can be described by the analytical expression for the z-component, derived in theory section, for small concentration gradients inside the linear response regime. The analytical expression can not be used outside this regime due to the fact that entrance effects give rise to a back flow into the channel at the lower concentration reservoir entrance and outside the linear regime this back flow is large enough to reverse the fluid flow.
The first priority in going further with research in this area is verifying the different linear response relations used. As it has been shown that that these relations have to hold for a cylindrical system in the considered regime [27], the verification is not impossible. Another aspect to look into is how the values on the channel axis can be described in an analytical manner. Furthermore an theory describing the entrance effects in the velocity field needs to be drawn up as these are the main contributor to the back flow which is created at the low concentration reservoir entrance. It is also interesting to look into the effects of a difference in mobility ($D_+ \neq D_=$) for the two ionic species considered, as equal mobility was assumed to simplify the complex system of a concentration gradient over a charged nanochannel.

7 Interests

There are no conflicts to declare.

References

[1] Wick, G.L. (1977) *Power from salinity gradients*. Energy, 1978.

[2] Bocquet,L.,& Tabeling, P. (2014). *Physics and technological aspects of nanofluidics*. Lab on a Chip, 2014.

[3] Alizadeh, A.,& Wang, M. (2018) *Reverse electrodialysis through nanochannels with inhomogeneously charged surfaces and overlapped electric double layer*.

[4] Rice, C.L.,& Whitehead, R. (1965) *Electrokinetic Flow in a Narrow Cylindrical Capillary*. The Journal of Physical Chemistry, 1965.

[5] Burgreen, D.,& Nakache, F.R. (1963) *Electrokinetic Flow in Ultrafine Capillary Slits1*. The Journal of Physical Chemistry, 1964.

[6] Ohshima, H.,& Kondo, T. (1989) *Electrokinetic flow between two parallel plates with surface charge layers: Electro-osmosis and streaming potential*. Journal of Colloid and Interface Science, 1990

[7] Pennathur, S.,& Santiago, J.G. (2005) *Electrokinetic Transport in Nanochannels. 1. Theory*. Analytical Chemistry, 2005.

[8] Yang, C.,& Li, D. (1997) *Analysis of electrokinetic effects on the liquid flow in rectangular microchannels*. Colloids and Surfaces A: Physicochemical and Engineering Aspects, 1998.

[9] Masliyah, J.H.,& Bhattacharjee, S. 2006 *Electrokinetic and Colloid Transport Phenomena*. Hoboken, NJ: John Wiley & Sons, Incorporated.

[10] Qian, S.,& Ai, Y. (2012) *Electrokinetic Particle Transport in Micro-/Nanofluidics: Direct Numerical Simulation Analysis*. Boca Raton, Fl: CRC Press

[11] Delgado, A.V. (2001) *Interfacial Electrokinetics and Electrophoresis*. Boca Raton, Fl: CRC Press

[12] Liu, X., Zeng, Q., Liu, C., Yanga, J.,& Wang, L. (2019) *Experimental and finite element method studies for femtomolar cobalt ion detection using a DHI modified nanochannel*. Analyst, 2019.

[13] Yan, F., Yao, L., Chen, K., Yanga, Q.,& Su, B. (2018) *An ultrathin and highly porous silica nanochannel membrane: toward highly efficient salinity energy conversion*. Journals of Materials Chemistry A, 2019

[14] Li-Chang Hung, L.,& Minh, M.N. (2015) *Stationary Solutions to the Poisson-Nernst-Planck Equations with Steric Effects*.

[15] Tagliazucchi, M.,& Szleifer, I. (2017) *Theoretical Basis for Structure and Transport in Nanopores and Nanochannels*. Chemically Modified Nanopores and Nanochannels (2017)

[16] Pilon, L., Wang, H.,& d'Entremont, A. (2014) *Recent Advances in Continuum Modeling of Interfacial and Transport Phenomena in Electric Double Layer Capacitors*. Journal of The Electrochemical Society, 2015.

[17] Van Roji, R. (2019) *Soft Condensed Matter Theory*.

[18] Constantin, P.,& Ignatova, M. (2018) *On the Nernst-Planck-Navier-Stokes system*. Archive for Rational Mechanics and Analysis, 2019.

[19] Gray, C.G.,& Stiles, P.J. (2018). *Nonlinear Electrostatics. The Poisson-Boltzmann Equation*. European Journal of Physics, 2018.

[20] Yuan, Z., Garcia, A.L., Lopez, G.P.,& Petsev, D.N. (2006) *Electrokinetic transport and separations in fluidic nanochannels*. Electrophoresis, 2007.

[21] Bagotsky, V.S.,& Mueller, K. (2005) *Fundamentals of Electrochemistry*, 2nd Edition. Hoboken, NJ: John Wiley & Sons, Incorporated.

[22] D'yachkov, L.G. (2004) *Analytical Solution of the Poisson–Boltzmann Equation in Cases of Spherical and Axial Symmetry.* Technical Physics Letters,2005.

[23] Outhwaite, C.W., Bhuiyan, L.B.,& Levine, S. (1979) *Theory of the electric double layer using a modified poisson–boltzman equation.* Journal of the Chemical Society Faraday Transactions, 1980.

[24] Prieve, D.C, Anderson, J.L.,& Ebel, J.P.,& Lowell, M.E. (1982) *Motion of a particle generated by chemical gradients. Part 2. Electrolytes.* Journal of Fluid Mechanics, 1984.

[25] Malmberg, C.G.,& Maryott, A.A. (1955) *Dielectric Constant of Water from 0º to 100º C.* Journal of Research of the National Bureau of Standards, 1956.

[26] Debye, P.,& Hückel, E. (1923) *The theory of electrolytes. I. Freezing point depression and related phenomena.* Translated and Typeset by Braus, M.J. (2019)

[27] Werkhoven, B.L.,& Van Roji, R. (2019) *Coupled water, charge and salt transport in heterogeneous nanofluidic systems.*

[28] Dow, J.O. (1999) *Introduction to Problem Definition and Development.* A Unified Approach to the Finite Element Method and Error Analysis Procedures, 1999.

[29] Chakrabarty, A., Mannan, S.,& Cagin, T. (2016) *Finite Element Analysis in Process Safety Applications.* Multiscale Modeling for Process Safety Applications, 2016.

A Solution To The Poisson-Boltzmann Equation In Planar Geometry

The Poisson equation for the dimensionless potential ϕ for the situation of $x = R - r$ is given by

$$\frac{d^2\phi}{dx^2} = \kappa^2 \sinh(\phi(x)), \tag{34}$$

in which κ is given by

$$\kappa = \sqrt{\frac{2c^0 N_A e^2}{k_B T \varepsilon_0 \varepsilon_r}}, \tag{35}$$

with c^0 the ionic concentration at $x = R$, which is defined under the assumption that on the axis, far away from the charged wall, both of the ion concentrations are the same, $c^0(z) = c^0_+ = c^0_-$. To find the function which describes the potential ϕ, this second order derivative needs to be solved. To do this, the following mathematical identity is used

$$(\frac{d\phi}{dx})^2 \equiv 2 \int \frac{d^2\phi}{dx^2} d\phi. \tag{36}$$

It is easy to check that this is indeed equivalent by differentiating with respect to x. Substituting the Poisson-Boltzmann equation (Eq. 34) gives

$$(\frac{d\phi}{dx})^2 = 2\kappa^2 \int \sinh(\phi) d\phi = \kappa^2 (e^{\phi} + e^{-\phi} - 2), \tag{37}$$

in which the fact is used that by definition $\phi|_{x=R} = 0$. This can be rewritten by using another mathematical identity

$$\sinh^2 X = (\frac{e^X - e^{-X}}{2})^2 = \frac{e^{2X} + e^{-2X} - 2}{4}. \tag{38}$$

By taking the square root, it can be found that

$$\frac{d\phi}{dx} = -2\kappa \sinh \frac{\phi}{2}, \tag{39}$$

the decision to take the negative option is a result of the physical situation which is described. By introducing a new variable y which is defined by the following relation $y = e^{\frac{\phi}{2}}$ this new equation can be solved by substituting y:

$$\frac{d\phi}{dx} = \frac{2}{y}\frac{dy}{dx} = -\kappa(y - \frac{1}{y}), \tag{40}$$

which simplifies to

$$\frac{dy}{dx} = -\frac{\kappa}{2}(y^2 - 1). \tag{41}$$

A solution to this problem would entail y being given by

$$y = \frac{1 + \gamma_1 e^{Fx}}{1 + \gamma_2 e^{Fx}}, \tag{42}$$

with γ_1,γ_2,F to be determined variables independent of x. This would mean that

$$\frac{dy}{dx} = \frac{(\gamma_1 F - \gamma_2 F)e^{Fx}}{(1 + \gamma_2 e^{Fx})^2} = -\frac{\kappa}{2}\frac{(2\gamma_1 - 2B)e^{Fx} + (\gamma_1^2 - \gamma_2^2)e^{2Fx}}{(1 + \gamma_2 e^{Fx})^2}. \tag{43}$$

As a result, y can only be of that form as $\gamma_1 = -\gamma_2$ and $F = -\kappa$ due to the fact that the case $\gamma_1 = \gamma_2$ is not an option. The function $y = 1$ has no non-zero second-order differential equation. The function y can now be written as a function of one unknown variable $\gamma = \gamma_1$. The second boundary condition is used to determine γ. This boundary condition is a result of Gauss' law

$$G = \frac{d\phi}{dx}|_{x=0} = -\frac{e^2}{\varepsilon_0 \varepsilon_r k_B T}\frac{\sigma_e}{e}, \tag{44}$$

and describes the relation between the potential at the wall and the surface charge of the wall. As all of the exponents in y will be zero at $x = 0$, this boundary condition can be given by

$$G = -\kappa(\frac{1+\gamma}{1-\gamma} - \frac{1-\gamma}{1+\gamma}) = -\kappa\frac{4\gamma}{1-\gamma^2}. \tag{45}$$

This gives $\gamma = \frac{2\kappa}{G} \pm \sqrt{(\frac{2\kappa}{G})^2 + 1}$, and as $|\gamma| < 1$ the unique solution of the potential can be given as

$$\phi = 2\ln\frac{1+\gamma e^{-\kappa x}}{1-\gamma e^{-\kappa x}}, \tag{46}$$

with $\gamma = \frac{2\kappa}{G} - \sqrt{(\frac{2\kappa}{G})^2 + 1}$ and $\kappa = \sqrt{\frac{2c^0 N_A e^2}{k_B T \varepsilon_0 \varepsilon_r}}$. Using the fact that $x = R - r$ this can be substituted again to give the potential depending on r,

$$\phi(r) = 2\ln\frac{1+\gamma e^{-\kappa(R-r)}}{1-\gamma e^{-\kappa(R-r)}}. \tag{47}$$

B Solution To The Fluid Velocity

The second partial differential equation of the fluid velocity is given by

$$\frac{\partial^2 u}{\partial r^2} = 2\frac{k_B T N_A}{\eta}\frac{\partial c^0}{\partial z}(\cosh\phi - 1). \tag{48}$$

As was done in the derivation of the solution to the dimensionless potential, the substitution $x = R - r$ is introduced. This gives a new partial differential equation for the fluid velocity in the z-direction,

$$\frac{\partial^2 u}{\partial x^2} = 2\frac{k_B T N_A}{\eta}\frac{\partial c^0}{\partial z}(\cosh\phi - 1). \tag{49}$$

This combined with the solution found for the dimensionless potential (Eq. 47) gives

$$\frac{\partial^2 u}{\partial x^2} = \frac{k_B T N_A}{\eta}\frac{\partial c^0}{\partial z}(\frac{4\gamma e^{-\kappa x}}{(1-\gamma e^{-\kappa x})^2} + \frac{-4\gamma e^{-\kappa x}}{(1+\gamma e^{-\kappa x})^2}), \tag{50}$$

where is used that

$$2(\cosh\phi - 1) = \frac{(1+\gamma e^{-\kappa x})^2}{(1-\gamma e^{-\kappa x})^2} + \frac{(1-\gamma e^{-\kappa x})^2}{(1+\gamma e^{-\kappa x})^2} - 2 = \frac{4\gamma e^{-\kappa x}}{(1-\gamma e^{-\kappa x})^2} + \frac{-4\gamma e^{-\kappa x}}{(1+\gamma e^{-\kappa x})^2}. \tag{51}$$

Keeping in mind that

$$f(y) = \frac{1}{1+Be^{-\kappa y}} \rightarrow f'(y) = \frac{B\kappa e^{-\kappa y}}{(1+Be^{-\kappa y})^2}, \tag{52}$$

simple integration of both sides gives

$$\frac{\partial u}{\partial x} = \frac{-4k_B T N_A \kappa}{\eta}\frac{\partial c^0}{\partial z}(\frac{1}{1-\gamma e^{-\kappa x}} + \frac{1}{1+\gamma e^{-\kappa x}} + 2 + C_1), \tag{53}$$

with C_1 an integration constant independent of x (it may depend on z).
Using the fact that

$$\frac{1}{1-\gamma e^{-\kappa x}} + \frac{1}{1+\gamma e^{-\kappa x}} = \frac{2}{1-\gamma^2 e^{-2\kappa x}} = \frac{2e^{2\kappa x}}{e^{2\kappa x} - \gamma^2}, \tag{54}$$

combined with

$$f(y) = \ln(e^{2\kappa x} - \gamma^2) \rightarrow f'(y) = \frac{2\kappa e^{2\kappa x}}{e^{2\kappa x} - \gamma^2}, \tag{55}$$

and

$$\ln(e^{2\kappa x} - \gamma^2) = \ln(1 - \gamma^2 e^{-2\kappa x}) + 4\kappa x, \tag{56}$$

The fluid velocity can be given as

$$u = \frac{-4k_B T N_A \kappa^{-1}}{\eta}\frac{\partial c^0}{\partial z}(\kappa^{-1}\ln(1-\gamma^2 e^{-2\kappa x}) + (2 + 4 + C_1)x + C_2), \tag{57}$$

with C_2 another integration constant independent of x. The boundary condition for C_1 is taken such that the linear x term disappears, as the fluid velocity outside the electric double layer is constant, as there is no potential for the concentration gradient to induce a fluid flow. The second boundary condition which needs to be taken into account is the no-slip boundary $u = 0$ at $x = 0$ (on the channel wall) is used to determine C_2. This enables the rewriting of the fluid velocity to

$$u(x) = \frac{-4k_B T N_A \kappa^{-2}}{\eta}\frac{\partial c^0}{\partial z}\ln\frac{1-\gamma^2 e^{-2\kappa x}}{1-\gamma^2}. \tag{58}$$

The fluid velocity in the z-direction depending on r is found can be found with the use of the substitution $x = R - r$,

$$u(r) = \frac{-4k_B T N_A \kappa^{-2}}{\eta}\frac{\partial c^0}{\partial z}\ln\frac{1-\gamma^2 e^{-2\kappa(R-r)}}{1-\gamma^2}. \tag{59}$$

C Begin Phase Numerical Study

In the begin phase of the numerical aspect of this study, a lot of time was spent on reproducing a cylindrical nanochannel with a pressure gradient instead of a concentration gradient. It falls a bit outside the scope of this paper, however it is important to understand the reasoning behind this earlier recreation. Compared to the concentration gradient system, the pressure system is far better understood. This is due to the fact that the pressure gradient is constant over the channel and the Debye length describing the electric double layer doesn't depend on the radial position r and axial position z. As a result this pressure system is less complex and therefore uses less computing power and time when computed numerically. As there was no earlier experience with the modelling program *COMSOL Multiphysics*, it seemed logical to start with this as both a means to gain experience with *COMSOL Multiphysics* and to remove errors easier (to estimate, a pressure system calculation took around 5 minutes, while a diffusio-osmotic system calculation often took over an hour). A lot of the evaluation of the mesh sizes with respect to efficiency (a decision between a better approximate solution and less computing time and power) was done in this earlier stage. This pressure system was checked for both linear response theory for pressure gradients and the Poisseuille flow (which describes the axial velocity for pressure gradients). After this, the pressure system was rebuild to the chemical gradient system, which is discussed in here discusses. For anyone using *COMSOL Multiphysics* to numerically calculate the diffusio-osmotic system, We encouraged to look into the pressure driven system first.